Chemical diffusivity and wave propagation in surface reactions: Lattice-gas model mimicking CO-oxidation with high CO-mobility

M. Tammaro and J. W. Evans

Citation: The Journal of Chemical Physics **108**, 762 (1998); doi: 10.1063/1.475436
View online: http://dx.doi.org/10.1063/1.475436
View Table of Contents: http://scitation.aip.org/content/aip/journal/jcp/108/2?ver=pdfcov
Published by the AIP Publishing

Chemical diffusivity and wave propagation in surface reactions: Lattice-gas model mimicking CO-oxidation with high CO-mobility

M. Tammaro
Ames Laboratory and Department of Physics, Iowa State University, Ames, Iowa 50011

J. W. Evans
Ames Laboratory and Department of Mathematics, Iowa State University, Ames, Iowa 50011

(Received 15 May 1996; accepted 3 October 1997)

We analyze the spatiotemporal behavior in a lattice-gas model for the monomer-dimer reaction on surfaces. This model, which mimics catalytic CO-oxidation, includes a *mobile* monomer adspecies (representing CO), an *immobile* dissociatively adsorbed dimer species (representing O), and a *finite* reaction rate (for CO_2 production). We characterize in detail the propagation of the chemical wave or reaction front produced when the stable reactive steady-state of the model displaces the metastable CO-poisoned state. In the regime of high CO-mobility, such propagation can be described directly within a ''hydrodynamic'' reaction-diffusion equation formalism. However, we show that the chemical diffusivity of CO is dependent on the O coverage, reflecting the percolative nature of CO-transport through a background of immobile O. We also emphasize that gradients in the coverage of immobile O induce a diffusive flux in the highly mobile CO. These features significantly influence wave propagation and reaction front structure. In addition, our analysis accounts for the feature that in this hydrodynamic regime, correlations persist in the distribution of adsorbed immobile O, and that these influence the reaction kinetics, the steady states, and the percolation and diffusion properties. To this end, we utilize a ''hybrid'' approach which incorporates a mean-field reaction-diffusion treatment of adsorbed CO, coupled with a lattice-gas treatment of adsorbed O [Tammaro *et al.*, J. Chem. Phys. **103**, 10277 (1995)]. © *1998 American Institute of Physics.* [S0021-9606(98)51402-X]

I. INTRODUCTION

Surface reactions on single-crystal substrates, under ultrahigh vacuum conditions, exhibit a rich variety of spatiotemporal behavior.[1] Traditionally, such behavior is described by mean-field (MF) reaction-diffusion equations with Fickian diffusion and coverage-independent chemical diffusion coefficients, D.[1] This approach ignores correlations or ordering in the adlayer, which result primarily from interactions between adspecies, but also from multisite adsorption, desorption, and reaction processes in the case of limited adspecies mobility. These effects clearly influence the nonlinear reaction kinetics and the steady-state coverages.[2] However, they also influence the chemical diffusion of adspecies, which controls the chemical wave propagation and spatial pattern formation in these systems. Furthermore, here we also emphasize that the traditional MF treatments ignore the feature that chemical diffusion occurs in *mixed* adlayers, where diffusion is intrinsically coverage dependent due to the influence of coadsorbed adspecies.

These complicating features of adlayer ordering and fluctuations, and of mixed adlayers, can in fact be treated within atomistic lattice-gas (LG) models.[2–6] Indeed, LG models have been applied to study a range of two-dimensional (2D) reaction systems. However, most such studies have *not* realistically treated surface reactions. Apart from simplifying assumptions regarding the reaction mechanism, the neglect of adspecies interactions (and thus the simplistic choice of coverage-independent rates for various adsorption, desorption, and reaction processes), the crucial role of the high mobility of some adspecies has generally *not* been appreciated or incorporated into the models. Indeed, hop rates for the most mobile adspecies are often many orders of magnitude larger than *all* other rates (including that for reaction).[7] This feature effectively eliminates the spatial correlations due to multisite adsorption, desorption, and reaction processes, and leads to local equilibration of such mobile adspecies (so that spatial correlations are determined by the adspecies interactions). Clearly, high mobility also results in the mixed adlayers, mentioned above. However, there are also more subtle effects. High mobility quenches fluctuations that produce transitions between distinct steady state ''branches,'' should they exist.[6,8] This results in the strong metastability and hysteresis often observed in experiments, and characteristic of mean-field treatments. Finally, we note that high mobility also determines the mesoscopic length scale, $L \sim (D/k_c)^{1/2}$, of the spatial patterns, and the ''large'' wave propagation velocities, $V \sim (k_c D)^{1/2}$, observed in these systems.[1] Here k_c is an effective rate for the overall reaction process, and D represents an effective diffusion coefficient, as above.

Our focus here is on chemical diffusion and spatiotemporal behavior in a simplistic LG reaction model for CO-oxidation, with highly mobile adsorbed CO, and immobile adsorbed O. The model supports a state of high reactivity with low CO coverage, for lower CO partial pressures (P_{CO}), as well as a completely poisoned CO-covered state. As P_{CO} increases above a critical value, P^*, the reactive state changes from stable to metastable, and the opposite

 0021-9606/98/108(2)/762/12/$15.00

occurs for the poisoned state. Fluctuations then induce a discontinuous transition from the reactive state to the poisoned state. We focus on the evolution of an interface between the reactive state and the poisoned state. For example, when $P_{CO} < P^*$, the stable reactive state displaces the metastable poisoned state leading to chemical wave propagation. As indicated above, high CO mobility quenches fluctuations, increasing the lifetime of the metastable states, and thus producing mean-field type bistability and deterministic wave propagation. However, despite the realization of mean-field type behavior in this regime, chemical diffusion coefficient, D_{CO}, of adsorbed CO is *not* necessarily coverage independent. One can only say that D_{CO} will be proportional to the hop rate for adsorbed CO. In this work, we fully characterize the nontrivial nature of chemical diffusion, and note the consequences for wave propagation.

First, in Sec. II, we describe in detail the LG monomer–dimer reaction model mimicking CO-oxidation on surfaces. We also present simulation results for this model, focusing on the propagation of chemical waves. Then, in Sec. III, we provide some general remarks concerning chemical diffusion. We describe effective diffusivity for finite CO-mobility, and give an explicit prescription for diffusion coefficients in the ''hydrodynamic'' regime of high CO-mobility. A direct analysis of spatiotemporal behavior in the hydrodynamic regime is presented in Sec. IV, and results are compared with those in Sec. II. This analysis is achieved by implementing a recently developed ''hybrid'' treatment which combines MF reaction-diffusion equations to describe the highly mobile adsorbed CO, coupled with a LG treatment of coadsorbed immobile O. In Sec. V, we discuss the limitations of the model, and notes refinements needed to facilitate comparison with experiment. Some final remarks are provided in Sec. VI.

II. LATTICE-GAS MODEL MIMICKING CO-OXIDATION ON SURFACES

A. Description of the monomer-dimer reaction model

The lattice-gas (LG) monomer–dimer surface reaction model, mimicking CO-oxidation, includes the following simple steps: CO(gas) adsorbs on single empty sites at rate p_{CO}; O_2(gas) adsorbs dissociatively on adjacent empty sites at rate p_{O_2}; adjacent CO(ads) and O(ads) react to form the product CO_2(gas) at rate k, leaving two empty surface sites. In addition, CO(ads) can hop to each adjacent empty site at rate h. These steps are summarized schematically as

$$\mathrm{CO(gas)}+E \xrightarrow{p_{CO}} \mathrm{CO(ads)}, \quad \mathrm{O_2(gas)}+2E \xrightarrow{p_{O_2}} 2\mathrm{O(ads)},$$

$$\mathrm{CO(ads)}+\mathrm{O(ads)} \xrightarrow{k} \mathrm{CO_2(gas)}+2E,$$

and

$$\mathrm{CO(ads)}+E \xrightarrow{h} E+\mathrm{CO(ads)}.$$

Here ''gas'' denotes gas phase species, ''ads'' adsorbed species, E an empty surface site, and $2E$ an adjacent empty pair. The impingement rates, p_{CO} and p_{O_2}, for CO(gas) and O_2(gas), respectively, are simply related to the partial pressures for these species; k denotes the reaction rate for each adjacent pair of CO(ads) and O(ads). Henceforth, we normalize the impingement rates such that $p_{CO}+p_{O_2}=1$, and we set $k=1$. Adspecies interactions, other than reaction of adjacent CO(ad) and O(ad), are ignored. The model is implemented on a square lattice of adsorption sites.

Some previous discussion of this model can be found in Refs. 4, 5 for $h=0$, and Refs. 8, 9 for $h>0$. We are primarily interested in the regime where $h \gg 1$, corresponding to the typical experimental situation where the CO(ads) hop rate, h, is many orders of magnitude larger than the other rates. With this in mind, it is appropriate to emphasize that we have chosen k *finite* here, rather than infinite (instantaneous reaction), as in several other studies.[3,6,10] Choosing infinite k does not qualitatively change the steady-state behavior or kinetics for spatially uniform systems. However, in the $h \to \infty$ limit for models with infinite k, only one reactant can have nonzero local coverage at a macroscopic point,[11] and this produces an artificial situation with regard to chemical diffusion and wave propagation (see Appendix A).

B. The discontinuous CO-poisoning transition

The key feature of the monomer–dimer reaction model of interest here is the occurrence of a discontinuous phase transition from a stable reactive steady-state to a stable CO-poisoned ''absorbing'' state, with increasing p_{CO}. The location of the transition is denoted by $p_{CO}=p^*$, where $p^*=p^*(h)$ depends on h. A metastable extension of the reactive state also exists for $p^* < p_{CO} < p_{s+}$, where $p_{s+}=p_{s+}(h)$ denotes an ''upper spinodal.'' Correspondingly, a metastable CO-poisoned state exists for some range $p_{s-} < p_{CO} < p^*$, where $p_{s-}=p_{s-}(h)$ denotes a ''lower spinodal.'' Clearly, because of its ''absorbing'' nature, the CO-poisoned state exists as a steady-state for all p_{CO}. It is stable for $p_{CO} > p^*$, metastable for $p_{s-} < p_{CO} < p^*$, and unstable $p_{CO} < p_{s-}$.[6]

As could be anticipated from the general discussion in Sec. I of the effect of diffusion on metastability,increasing h in this monomer–dimer reaction model leads to an increase in the lifetime of the metastable states. In fact, it also greatly broadens their existence range.[6,8,9,11] For example,in our model with $k=1$, the width of the existence region for the metastable reactive state increases dramatically from 0.005,

TABLE I. Dependence of the location, $p^*(h)$, of the discontinuous poisoning transition on the CO(ads) hop rate, h, for the LG monomer–dimer surface reaction model with $k=1$.

h	p^*
0	0.4328
1	0.4227
4	0.4152
16	0.4070
32	0.4044
64	0.4027
∞	0.397

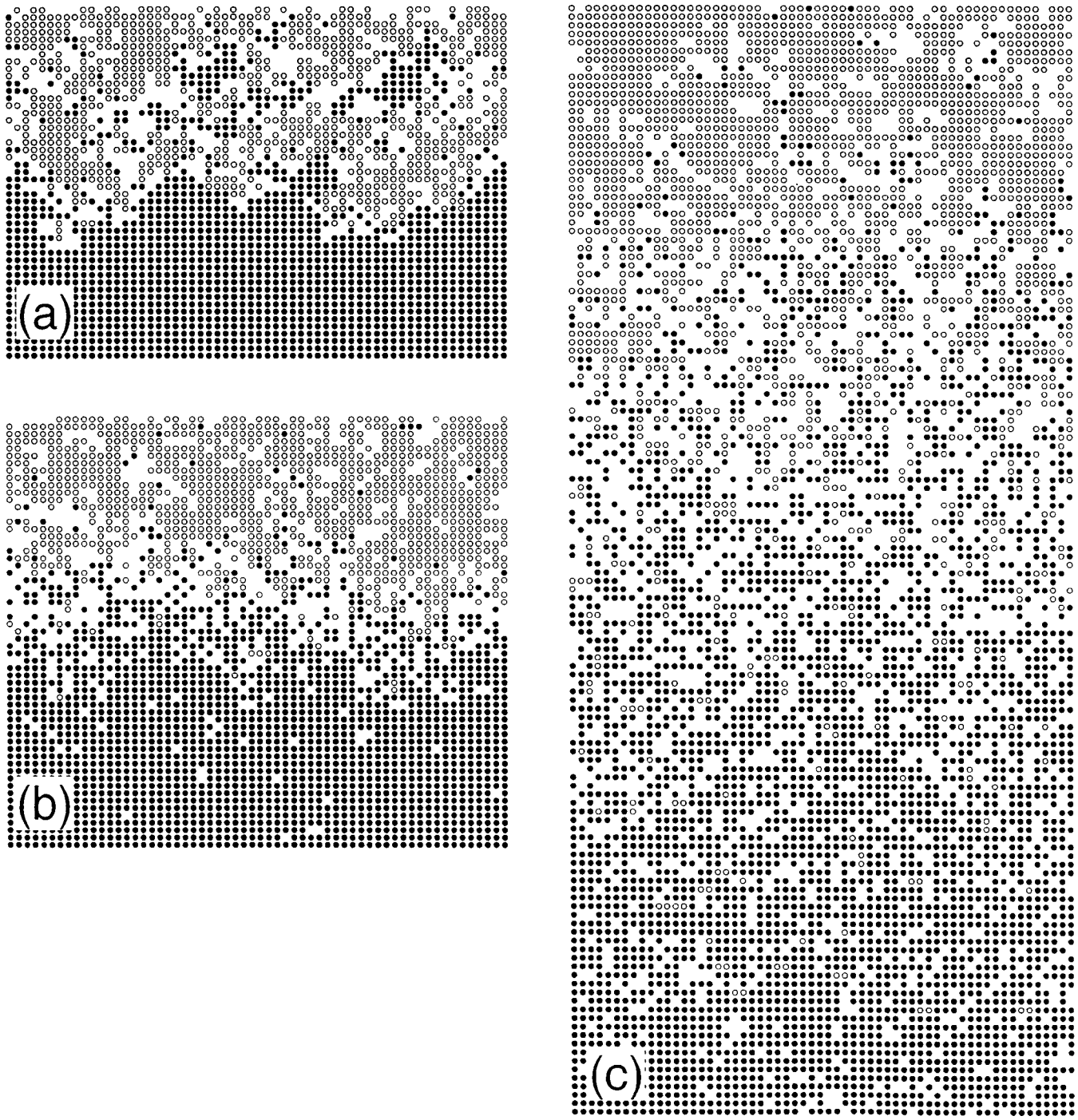

FIG. 1. Simulated configurations for cuts through the interface between the reactive steady-state (on the top) and the CO-poisoned state (on the bottom) at the discontinuous transition, $p_{CO}=p^*(h)$, for (a) $h=0$; (b) $h=16$; (c) $h=512$. Mobile CO(ads) is represented by ●, and immobile O(ads) by ○.

when $h=0$, to 0.103, when $h\to\infty$. More specifically, one finds that $p^*(0)=0.432$ and $p_{s+}(0)=0.437$,[5] whereas $p^*(\infty)\approx 0.397$ (see below) and $p_{s+}(\infty)\approx 0.500$.[8] One ramification is that determination of the location of the poisoning transition by monitoring the kinetics for various p_{CO} (and noting the onset of poisoning) tends to overestimate p^*, since the system gets trapped in the metastable reactive state for p_{CO} slightly above p^*.[11] Such corrupted estimates can be avoided either by performing an appropriate ''epidemic analysis,'' [5] or by implementing the ''constant-coverage ensemble'' method.[12] Estimates for p^* vs h from the latter approach are reported in Table I.[13]

C. Propagation velocity of the chemical wave

The chemical waves analyzed here are produced, for $p_{CO}\lesssim p^*(h)$, when the stable reactive steady-state *displaces* the metastable or unstable CO-poisoned state, which is separated from it by an on-average planar interface (see Fig. 1). This phenomena was noted in the original paper of Ziff

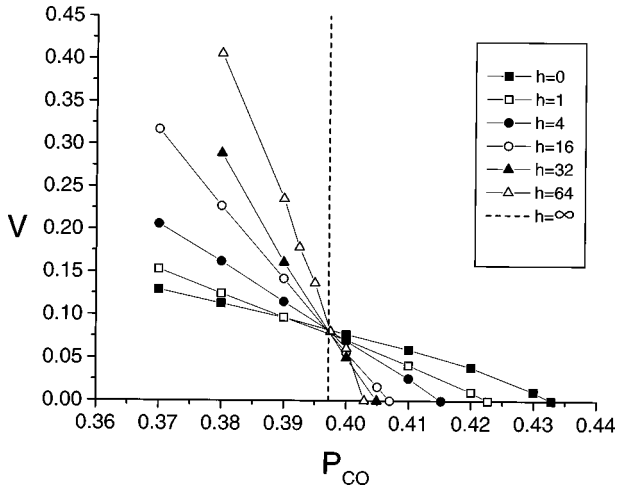

FIG. 2. Chemical wave propagation velocity, V, vs p_{CO} (below p^*), for various h (shown). The dashed vertical line shows limiting behavior for $h \to \infty$.

et al.[3] on the monomer–dimer model with infinite k, and $h=0$ (the so-called ZGB model). It has been studied in detail more recently for extensions of the ZGB model including adspecies diffusion.[6,10] One expects that for our model with $k=1$, and any *fixed* h, the propagation velocity, V, vanishes linearly with $\Delta = p^* - p_{CO} \geqslant 0$,as $\Delta \to 0$. This is due to the disappearance of the driving force for the reactive state to displace the CO-poisoned state on approaching the transition.[14] It is also appropriate to consider the dependence of V on h, for *fixed* Δ. One can argue that V should scale like L_c/τ_c, where $\tau_c = 1/k_c = O(1)$ is a characteristic time for the reaction process, and L_c is an overall characteristic length. L_c is determined by both the diffusion length, $L_d \sim \tau_c h^{1/2}$, and a ''direct spatial coupling'' length, $L_r = O(1)$, due to reaction between distinct adspecies at neighboring sites. (Here, all distances are measured in units of the lattice constant.) Consideration of generalized spatial contact models[15] for spreading or propagation due to both direct spatial coupling or contact, as well as due to conventional diffusion, suggests that $L_c^2 \approx L_r^2 + L_d^2$.[6] Together, the above observations imply that[6]

$$V \approx A(B+h)^{1/2}\Delta, \tag{1}$$

at least for large h, and small Δ. By comparison with conventional mean-field reaction-diffusion equation analyses, where $V \sim (k_c D)^{1/2}\Delta$,[1] one might define an effective diffusion coefficient, D_{eff}, in context of chemical waves, which scales like $D_{\text{eff}} \sim A^2(B+h)$. See also Ref. 10 and Sec. III.

The behavior described above was indeed observed using conventional Monte Carlo simulations to determine V as a function of $p_{CO} \leqslant p^*(h)$, for various choices of $h \geqslant 0$. The results are shown in Fig. 2. Here V is determined from the variation of the location of the interface defined as in Ref. 8. Of course, various definitions of this location are possible, but all give the same V for steady-state propagation. Uncertainties are negligible for larger V, and increase up to 10% for smaller V. First, we note that the values of the impingement rates, p_{CO}, where $V=0$, coincide exactly with the p^*-values determined independently above from the constant-coverage ensemble method. However, the most dramatic feature apparent in Fig. 2 is the ''near-crossing'' of curves for different h, which occurs at $p_{CO} = p_x = 0.397 \pm 0.002$ and $V = V_x \approx 0.08$. This type of behavior is certainly consistent with Eq. (1), which shows that the slope of such curves must diverge, as $h \to \infty$. Perhaps, most importantly, one can conclude from Eq. (1) that the ''crossing point'' yields an estimate of

$$p^*(h \to \infty) = p_x = 0.397 \pm 0.002, \quad \text{when} \quad k=1. \tag{2}$$

In this way, simulations for a range of ''small'' h can be reliably extrapolated to assess limiting behavior of $p^*(h)$, in the physically relevant regime of very large h.

One can also extract from this simulation data estimates for the values for the parameters, A and B, in Eq. (1). This is most naturally achieved by examining the quasilinear variation with h of $(dV/d\Delta)^2 \approx D_{\text{eff}} \approx A^2(B+h)$, in the regime of *large* h. From this behavior using values for $dV/d\Delta$ at the crossing-point for large h, we find that $A = 2.2 \pm 0.3$ and a B-value of order unity.

Finally, we note that analogous ''near-crossing'' behavior of V vs p_{CO} curves, for various h, was observed previously by Goodman *et al.*[10] for the monomer–dimer reaction model with *infinite* k (instead of $k=1$), but retaining mobile CO with hop rate h, and immobile O (see Appendix A).

D. Structure of the chemical wave front

We now discuss in more detail the structure of the chemical wave front. From Fig. 1, it is apparent that there are fluctuations in the location of the interface between the reactive and CO-poisoned states, and that these are particularly dramatic for small h. The total amplitude of these fluctuations, ξ, is naturally decomposed into contributions due to *intrinsic fluctuations*, ξ_i, and due to *long-wavelength fluctuations*, ξ_0, where $\xi^2 \approx \xi_i^2 + \xi_0^2$.[6,16] For $h=0$, large intrinsic fluctuations occur when $p_{CO} = p^*$ [and these are the dominant feature in Fig. 1(a)], although they are significantly reduced when $p_{CO} < p^*$. Figure 1 also indicates that increasing h above zero, when $p_{CO} = p^*$, quenches the intrinsic fluctuations[6] (or at least they do not grow significantly, depending on the precise definition of the interface location, and of ξ_i). However, they are expected to increase slowly with larger h. For example, ''diffusion front'' studies suggest that $\xi_i \sim h^{2/7}$, if one defines the interface as the ''shoreline'' of the CO-covered region (see Appendix B).

It has also been shown[6,10] that the long-wavelength fluctuations are described by the stochastic KPZ-equation,[17] for $p_{CO} < p^*$. As a result, the amplitude of these fluctuations, measured over a locally-equilibrated section of the interface of length L, must scale like $\xi_0 \approx 24^{-1/2}(\gamma L/\nu)^{1/2}$, where γ measures the amplitude of the shot-noise in the KPZ equation, and ν denotes the kinetic surface tension at the interface.[10,17] Comparison of KPZ and mean-field reaction-diffusion equation analyses of the evolution of curved interfaces indicates that $\nu \sim h$, for large h.[6] This increase in the kinetic surface tension with h quenches the long-wavelength

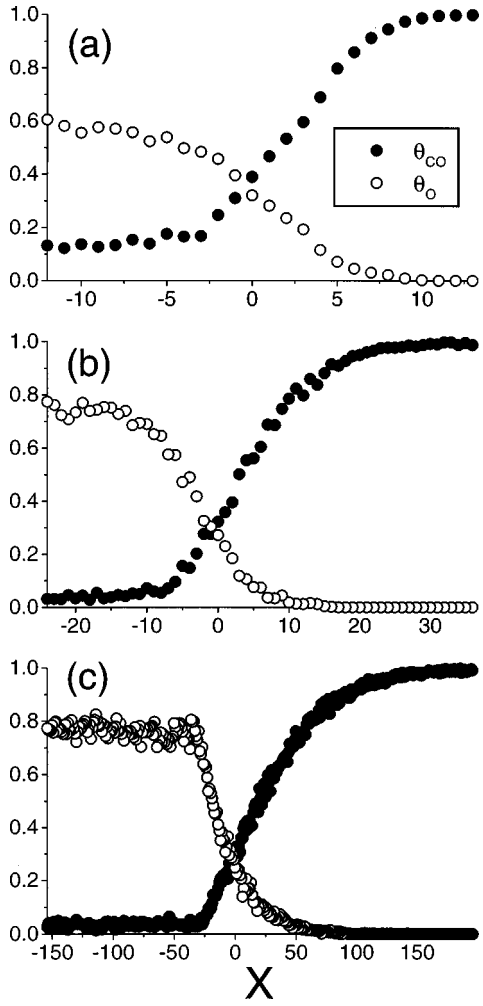

FIG. 3. Simulated coverage profiles across the interface between the reactive steady-state (on the left) and the CO-poisoned state (on the right) at the discontinuous transition, $p_{CO}=p^*(h)$, for (a) $h=0$; (b) $h=16$; (c) $h=512$. The position x is given in units of lattice constants. The length, Δx, of profile shown is chosen as the same fixed multiple of $L_c \propto A(B+h)^{1/2}$, for each h-value [specifically, $\Delta x \approx 7A(B+h)^{1/2}$, with $A=2.2$ and $B=1.8$].

fluctuations. Thus, for example, one has $\xi_0 \sim \gamma^{1/2} h^{-1/4}$, on the characteristic length scale, $L \sim L_c \sim h^{1/2}$, for large h. Finally, we note that while the long-wavelength fluctuations are not of the KPZ type precisely at the transition,[6,10] it is clear that they are still quenched with increasing h.

The key observation from the above analysis is that all fluctuations ''quickly'' become insignificant relative to the characteristic length scale, $L_c \sim h^{1/2}$, with increasing h. This is entirely consistent with the general statements in Sec. I concerning the enhancement of metastability and the attainment of ''mean-field behavior,'' with increasing surface mobility (see Refs. 6, 8, 10, 11).

Finally, in Fig. 3, we show concentration profiles for cuts through the ''equilibrated'' reaction front at $p_{CO}=p^*$, obtained from simulations of systems with a fixed width of 600 lattice spacings. Here, θ_{CO} and θ_O denote the mean coverage of CO and of O, respectively, along rows of sites orthogonal to the direction of propagation. From these profiles, one can clearly see the increase with h of the ''characteristic width'' of the front (which corresponds to L_c). The smooth nature of the profile for $h=0$ in Fig. 3(a), and the primary contribution to the width, come from the intrinsic fluctuations. Also, examining the evolution of the shape of the profiles with increasing h [Figs. 3(a)–3(c)] one anticipates the development of a nonanalytic form in the $h \to \infty$ limit. This form is quite distinct from typical chemical wave profiles derived from conventional reaction-diffusion equations with constant diffusion coefficients.[18] Indeed, we shall show in Sec. IV that the unusual form in this model is associated with the percolative nature of CO-diffusion.

III. CHEMICAL DIFFUSION

Here we first consider, in general, mixed adlayers, where a mobile species, CO(ads), which hops to adjacent empty sites, coexists with an immobile species, O(ads). In the hydrodynamic regime of high CO-mobility, chemical diffusion is described in terms of the diffusive mass flux, J_{CO}, of CO(ads) across the surface generated by spatially nonuniform coverages. We emphasize that a flux, J_{CO}, can be generated both by gradients in the CO-coverage, and in the O-coverage, so one writes

$$\vec{J}_{CO} = -D_{CO,CO} \nabla \theta_{CO} - D_{CO,O} \nabla \theta_O \tag{3}$$

for small gradients. The coefficients $D_{CO,CO}$ and $D_{CO,O}$ are not generally constant and below we explicitly determine their coverage dependence. We note that diffusion is not possible for when $\theta_{CO}+\theta_O=1$, then since here $\Delta\theta_{CO}=-\Delta\theta_O$, it follows immediately that $D_{CO,CO}$ and $D_{CO,O}$ must be equal for such a ''jammed'' surface.

For general lattice-gas models involving surface diffusion of *all* adspecies, a unique relationship of the form (3) between flux and coverage gradients only exists in the hydrodynamic regime of high mobility. Here, the diffusion coefficients are determined by the partial coverages (and substrate temperature), which determine the unique locally equilibrated steady state of the adlayer. (We do however emphasize that these coefficients depend on the spatial correlations within this state.)[19] For our model, the situation is actually more complicated since in the locally ''equilibrated'' state, the distribution of immobile O(ad) depends on the history of formation of that state, rather than just on the coverages. However, some simplification occurs in our study of steady-state chemical wave propagation, since there is in fact a unique local reactive state for each point across the wave front. Finally, we note that in addition to studies of the hydrodynamic regime, directly below we also consider the case of finite mobilities, where there is some basis for the definition of an effective chemical diffusivity.

A. Effective chemical diffusivity for finite mobility

From examination of exact master equations for our LG surface reaction model with finite h for spatially nonuniform system, it is clear that spatial nonuniformities produce a diffusive flux of CO. For a square lattice, with sites labeled (i,j), suppose that one has translational invariance in the j-direction. Then let $[O_i]$ denote the mean O-coverage in

column ''i,'' let $[E_iO_{i+1}]$ denote the probability of an adjacent empty site in column ''i'' and O-occupied site in column ''$i+1$,'' etc. Then the net diffusive flux of CO(ad) from column ''i'' to column ''$i+1$'' has the form[8]

$$\begin{aligned} J_{CO}(i\to i+1) &= h([CO_iE_{i+1}]-[E_iCO_{i+1}]) \\ &= -h([CO_{i+1}]-[CO_i]) \\ &\quad + h([O_iCO_{i+1}]-[CO_iO_{i+1}]). \end{aligned} \tag{4}$$

Now, one has $aJ_{CO}(i\to i+1)\to(\vec{J}_{CO})_x$, $a^2h\to D^0$ (the CO-diffusion coefficient for vanishing coverages), and $a^{-1}([A_{i+1}]-[A_i])\to\partial/\partial x[A]$, for large h. Thus, if one *neglects* correlations in the occupancy of adjacent sites (so, e.g., $[O_iCO_{i+1}]=[O_i][CO_{i+1}]$), one obtains

$$(\vec{J}_{CO})_x \approx -D^0(1-\theta_O)\partial\theta_{CO}/\partial x - D^0\theta_{CO}\partial\theta_O/\partial x. \tag{5}$$

This expression has the qualitative form of Eq. (3) above, although we emphasize that it is not exact due to the neglect of spatial correlations (except when $\theta_O\to 0$; see Sec. III B).

From the simulation results of Sec. II, it is also clear that even in the absence of adspecies hopping, spatial nonuniformities can be removed, e.g., leading to wave propagation. This is a consequence of spatial coupling associated with nearest-neighbor adsorption site requirement for O_2, and the adjacent site requirement for reaction. The indirect adsorption-desorption (or reaction) pathway effectively produces a nondiffusive lateral flux of CO that is controlled by adsorption and reaction rates, and the range of the spatial coupling (here just one lattice spacing). As also noted in Sec. II, this phenomenon apparent in general spatial contact models,[15] where the equations governing spatiotemporal behavior can be rewritten in a reaction-diffusion form within the so-called ''diffusion approximation'' (which neglects spatial correlations). Formulations of this type for the spatially inhomogeneous monomer–dimer reaction can be found in Refs. 20, 21. These studies primarily utilize the simplest ''site-approximation'' which neglects all spatial correlations, suitably extending this approximation to spatially inhomogeneous systems. Generalization to more sophisticated ''dynamic cluster'' approximations for spatially inhomogeneous systems, which account for short range correlations, is straightforward.[4,20,21] However, such approximations generally *cannot* describe the nontrivial nature of chemical diffusion in mixed adlayers, for realistic large h. This is clearly the case for the model studied here where correct description of the percolative nature of diffusion requires a sophisticated characterization of the connectivity of non-O(ads) regions of the lattice (see below).

Chemical diffusion coefficients cannot be precisely defined for finite hop rates. Since there is not a complete separation of time scales for hopping (diffusion) and other processes, relaxation of weak perturbations of uniform states will be dominated by nondiffusive pathways. However, it is natural to define an effective chemical diffusivity based, e.g., on the type of wave propagation behavior described in Sec. II. Since true diffusion and adsorption-desorption mechanisms provide *parallel* pathways for spatial homogenization, the total effective diffusivity is given by sum of contributions from these pathways, as is already apparent in the identification of D_{eff} in Sec. II. However, we emphasize that the former contribution dominates in the hydrodynamic regime, which is relevant to realistic modeling of surface reactions.

B. Chemical diffusion in noninteracting lattice-gases

There is a special case where the analysis and properties of chemical diffusion are particularly simple, and which is of direct relevance to this study. This is the case of ''random diffusion'' of a noninteracting adspecies of finite coverage or ''density'' by hopping to adjacent vacant sites, either on a perfect lattice, or in a static disordered lattice where some sites are ''blocked.'' Here, it is known that the associated many-particle master equations describing diffusion reduce to single-particle diffusion equations.[22,23] An important consequence is that the chemical diffusion coefficient, D, is *independent* of the coverage of the diffusing species. Of course, the diffusion of a single particle and, thus, the diffusion of the non-interacting lattice-gas, depends on the details of disordered environment.

The key results relevant to our study can be extracted from analyses of transport in lattice percolation models where some fraction, q, of the lattice sites are ''impurities'' which block transport.[24] We apply these results to analyze transport of the highly mobile adspecies CO, where the ''impurities'' correspond to coadsorbed O. The basic feature of these models is that ''percolating clusters'' of neighboring vacant sites, which connect opposite sides of the system, exist only when q is *below* a critical threshold, q_c. Thus, for $q<q_c$, long-range diffusion (by hopping between adjacent vacant sites) is possible, and $D>0$. For $q>q_c$, no long-range diffusion is possible, and thus $D=0$. If we set $D=D^0$ when $q=0$, and write $D=D^0F_{perc}(q)$, then $F_{perc}(q)$ decreases from unity (when $q=0$) to zero (as q increases to q_c), and $F_{perc}(q)=0$, for $q\geqslant q_c$. We emphasize that the critical percolation threshold depends on spatial correlations in the distribution of the blocked sites. However, the nature of the nonlinear disappearance of $F_{perc}(q)\sim(q_c-q)^\mu$ upon approaching the critical threshold (from below) is described by a universal exponent $\mu\approx 1.3$.[24] We also note that most studies of percolation focus on connectivity of the occupied rather than the vacant sites. These are generally distinct problems,[25] one exception being the most commonly studied ''ideal case'' of randomly distributed blocked sites.

In this work, we shall also exploit another quantitative characterization of the dependence of D on q, which is provided by formal ''density'' expansion techniques.[26] These expansions are obtained by first developing an Ursell–Mayer cluster expansion for (a suitable transform of) the propagator for diffusion on a disordered lattice. The mth-order term in this cluster expansion involves only propagators for lattices with up to ''m'' impurities, and this determines the q^m-term in the expansion D, after appropriate ensemble average over relative positions of such finite subsets of impurities. To date, only the case of a *random distribution of impurities* has been considered, where such ensemble averages involve uni-

form sums over all relative positions of subsets of m impurities.[26] In particular, for a square lattice, such an analysis yields[26]

$$F_{\mathrm{perc}}(q)=1-(\pi-1)q-\alpha q^2+O(q^3), \tag{6}$$

where $\alpha\approx 0.855\,71$. The quadratic approximation to Eq. (6) reproduces simulation results with uniform accuracy, and produces an estimate for q_c of 0.4023 (corresponding to $D=0$), which should be compared with the exact value of 0.4073. Of course, this approximation produces $\mu=1$, rather than the correct nontrivial value, but this limitation is not important in the context of our studies.

From the above discussion, it is clear that the introduction of spatial correlations in the (static) distribution of impurities does not change the linear ''single impurity'' term in Eq. (6). However, the quadratic term is associated with sum over the relative position of pairs of impurities, which must now be weighted by the associated pair-probability distribution function (rather than being a uniform sum). Thus α is modified depending on this function. It is appropriate to note that this pair-probability distribution provides only somewhat indirect information on the percolation threshold, in contrast to the distinct pair-connectivity function.[24] Thus, one should not expect the quadratic approximation to Eq. (6), with appropriately calculated α, to accurately predict q_c in general. However, our strategy will be to use a quadratic approximation with α chosen to match independently determined q_c, and this expression is expected to uniformly approximate F_{perc}.

C. Chemical diffusion coefficients $D_{\mathrm{CO,CO}}$ and $D_{\mathrm{CO,O}}$

In our monomer–dimer reaction model, the disordered environment through which the highly mobile noninteracting CO(ads) diffuses is provided by the immobile coadsorbed O(ads). Since the CO(ads) hop rate is much higher than all other rates, this environment can be regarded as effectively static. The chemical diffusion coefficient, $D_{\mathrm{CO,CO}}$, will depend on the coverage *and* configuration of the coadsorbed O(ads), but *not* on θ_{CO}. Although, as noted above, the local state depends on its history of formation, rather than just on θ_{O}, it is instructive (but somewhat oversimplistic) to write

$$D_{\mathrm{CO,CO}}=D^0F_{\mathrm{perc}}(\theta_{\mathrm{O}}), \tag{7}$$

where again $D^0=a^2h$ is the CO-diffusion coefficient for vanishing coverages.

In analyzing the diffusive flux of CO(ads) induced by a gradient in the O(ads)-coverage, a key observation is that the many-particle master equations for the noninteracting CO lattice-gas still reduce to single-particle equations, even for a nonuniform disordered background. Thus, the induced flux must be directly proportional to the coverage of CO(ads), and one can write $D_{\mathrm{CO,O}}=D^0\theta_{\mathrm{CO}}G(\theta_{\mathrm{O}})$. Then the condition that $D_{\mathrm{CO,CO}}=D_{\mathrm{CO,O}}$ for a ''jammed'' surface, where $\theta_{\mathrm{CO}}+\theta_{\mathrm{O}}=1$, yields $G(x)=F_{\mathrm{perc}}(x)/(1-x)$, so

$$D_{\mathrm{CO,O}}=D^0\theta_{\mathrm{CO}}F_{\mathrm{perc}}(\theta_{\mathrm{O}})/(1-\theta_{\mathrm{O}}). \tag{8}$$

Below, we describe the prescription of Eq. (7) and Eq. (8) as percolative CO-diffusion.

IV. HYBRID TREATMENT OF THE HYDRODYNAMIC REGIME OF HIGH MOBILITY

A. The hybrid mean-field/lattice-gas formalism

In the regime of high CO mobility (i.e., very large h), the adsorbed CO are locally randomized in a quasistatic disordered environment of coadsorbed O. For this reason, it is natural to analyze *directly* this limiting behavior within a so-called ''hybrid'' formalism.[8,27] Here, the immobile O(ads) distribution is treated within a lattice-gas (LG) framework (just as in our simulations for finite h), but the CO(ads) is described by a single mean-field parameter, $\theta_{\mathrm{CO}}=\theta_{CO}(x,t)$, representing the local CO-coverage at a macroscopic point, x, at time t. For a spatially uniform system, where $\theta_{\mathrm{CO}}=\theta_{\mathrm{CO}}(t)$, analysis of this hybrid model reveals true bistability of reactive and CO-poisoned states over a range of p_{CO} from $p_{s-}=0$ to $p_{s+}=0.500$.[8] Such true bistability is expected since increasing h enhances metastability in the full LG model, as noted in Sec. I and II. We emphasize, however, that this hybrid model does *not* provide an exact analysis of $h\to\infty$ limiting behavior of the full LG model. For the latter, there are variations or fluctuations in the CO coverage on regions which are topologically disconnected by ''walls'' of O(ads). These fluctuations are not accounted for in the hybrid treatment. While there is no indication that they effect the qualitative behavior of the model, they could produce small quantitative changes.

In reality, h is finite, although typically very large. Thus local equilibration (i.e., randomization) of CO(ads) is efficient, but there can be variations of CO (and O) coverages on a mesoscopic length scale, $O(h^{1/2})$. This feature is manifested in experimentally observed wave propagation and pattern formation.[1] To treat such phenomena within the hybrid approach, one can simulate in *parallel* the state of distributed macroscopic points with distinct local coverages, using a LG description of O(ads), and a MF description of CO(ads), with θ_{CO} now representing the local coverage. One must also suitably couple the evolution at these distinct macroscopic points (and thus of the parallel simulations) to describe the macroscopic diffusive mass transport of CO(ads).[8] Within such a ''hydrodynamic'' reaction-diffusion formalism, it is necessary to *prescribe* the chemical diffusivity of CO(ads). The simplest approximation assumes a constant diffusion coefficient, and a modified treatment has been considered which accounts for the influence of coadsorbed species, but neglects all spatial correlations, i.e., using Eq. (5) for $\vec{J}_{\mathrm{CO}}$.[8] However, for the model under consideration here, the appropriate nontrivial prescription of percolative diffusion is given by Eqs. (7) and (8) in Sec. III C.

Below, we exploit this hybrid treatment of spatially inhomogeneous systems to analyze the evolution of planar chemical waves. Paralleling the study of Sec. II, we examine the displacement of the reactive steady-state by the CO-poisoned state, which occurs for p_{CO} below an *equistability point* in the bistability region. For p_{CO} above this equistabil-

ity point, the displacement would be reversed for constant D, but it is actually absent for percolative diffusion (see Sec. IV B). In any case, by scanning p_{CO} across the bistability region, one can determine the equistability point for these two states. The equistability point corresponds to, and thus provides a direct estimate of $p^*(h\to\infty)$, which was determined independently in Sec. II.[8,11]

B. Wave propagation with percolative diffusion: General properties

In the $h\to\infty$ limit, planar chemical wave propagation in the x-direction in our monomer–dimer reaction model is described by equations of the form[8]

$$\partial/\partial t\,\theta_{CO}=p_{CO}\theta_E-4k\,\theta_{O,CO}+\partial/\partial x[D_{CO,CO}\partial/\partial x\,\theta_{CO}]+\partial/\partial x[D_{CO,O}\partial/\partial x\,\theta_O],$$

and

$$\partial/\partial t\,\theta_O=2p_{O_2}\theta_{E,E}-4k\,\theta_{O,CO}. \tag{9}$$

Here θ_{CO}, θ_O, and $\theta_E=1-\theta_{CO}-\theta_O$ denotes the probability that a site is occupied by CO, O, or empty (E), respectively, $\theta_{O,CO}$ denotes the probability of finding an adjacent O–CO pair (as distinct from a CO–O pair), and $\theta_{E,E}$ denotes the probability of an adjacent empty pair. Since the CO(ads) are locally randomly distributed, one has $\theta_{O,CO}=\theta_{O,Z}\theta_{CO}/\theta_Z$ and $\theta_{E,E}=\theta_{Z,Z}(\theta_E/\theta_Z)^2$ where Z denotes a non-O site. We emphasize that since the O(ads), and thus the Z's, are not randomly distributed, these equations are not closed, and need to supplemented by an infinite hierarchy.[8] However, direct assessment of some of the properties of the solutions to Eq. (9) is still possible. For a chemical wave with velocity V in the x-direction, one has $\theta_{CO}=\theta_{CO}(\xi=x-Vt)$, etc., and the above equations (and their extended hierarchy) can be reduced to ordinary differential equations in the standard way upon making the replacements $\partial/\partial t\to -V\partial/\partial\xi$, $\partial/\partial x\to\partial/\partial\xi$.[18]

Consider first the case of p_{CO} *below* the equistability point (see Sec. IV A), so that a planar chemical wave can be formed in which the reactive state on the left, say, displaces the CO-poisoned state on the right. This corresponds to $V>0$. For our reaction model, θ_O in such a reactive state always exceeds the critical threshold, q_c, for the termination of CO-diffusion, and trivially $\theta_O=0$ in the CO-poisoned state. Thus, θ_O will decrease from above q_c, to below q_c, with increasing ξ. Consequently, we can assign $\xi=0$ to the point where $\theta_O=q_c$, so there is no CO-diffusion for $\xi<0$. Then, it is clear from the above equations that the profile shape for $\xi<0$ is simply determined by the time-trace (after the replacement $t\to x/V$) of the coverages in a uniform system relaxing from the state at $\xi=0$ to the reactive steady-state. For $\xi>0$, the profile depends on the form of $D_{CO,CO}$ and $D_{CO,O}$. One can show that when $V>0$, the profile is continuous, and there is no slope discontinuity at $\xi=0$ since $\mu>1$.[28] However, upon approaching the equistability point, where $V\to 0$, the profile develops a *discontinuity* at $\xi=0$: coverages approach their reactive steady-state values for all $\xi<0$, so $\theta_O\to$constant, strictly exceeding q_c; however, θ_O decreases from q_c to zero, for increasing $\xi\geqslant 0$. This behavior is indicated schematically in Fig. 4.

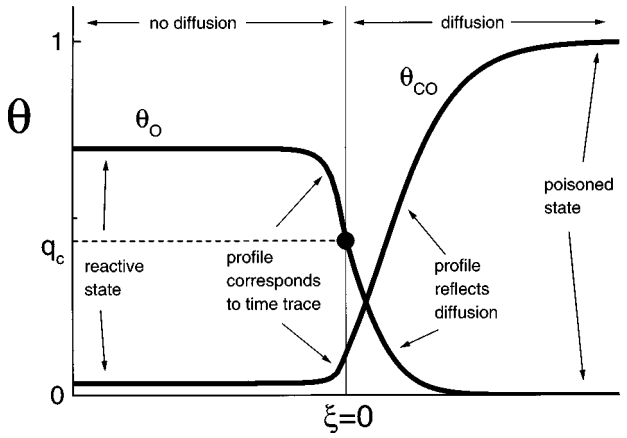

FIG. 4. Schematic of the chemical wave profile for p_{CO} slightly below p^*.

For p_{CO} *just above* the equistability point, propagation involving displacement of the reactive steady-state by the more stable CO-poisoned state does *not* occur in this hybrid formalism with percolative diffusion. This is because the reactive steady-state value of θ_O exceeds q_c, which precludes diffusive coupling of the CO-poisoned state to this reactive state. (However, as p_{CO} approaches the upper spinodal, the reactive steady-state value of θ_O drops below q_c, and again propagation occurs.) For completeness, in Appendix C, we indicate corresponding behavior in the LG model for p_{CO} just above p^*.

C. Wave propagation with percolative diffusion: Simulation results using the hybrid formalism

As an initial simplified treatment of wave propagation within the hybrid formalism, we assume that the ''weak'' correlations in the distribution of adsorbed O do not affect the percolation or transport properties for diffusing CO(ads). In this case, to describe chemical diffusion of CO(ads), one might use Eqs. (7) and (8) with a quadratic approximation for F_{perc}, where we slightly adjust the exact value for α,[26] so that we recover exactly the random percolation threshold of $q_c=0.4073$. With this choice, we determine that the equistability point for the reactive and CO-poisoned states occurs at $p_{CO}\approx 0.395\pm 0.001$.

Next, we implement a self-consistent treatment of percolation and transport within the hybrid formalism, as follows. In the above analysis of wave propagation near the equistability point, one can analyze the simulated distributions of adsorbed O across the wave front to assess at what position (and, thus, at what value of θ_O) the non-O(ads) sites cease to percolate. Specifically, we use small-cell real-space renormalization group techniques[29] to estimate the *shift* in the percolation threshold from its value for a random distribution. See Appendix D for more details. From this analysis, one finds that the percolation threshold is shifted upward by $\delta\approx 0.028$ from $q_c=0.4073$, for a random distribution, to q_c

TABLE II. Estimates for the location of the equistability point, p^*, of the monomer–dimer model in the hydrodynamic regime. Results are shown for simulations of the hybrid model (simulation) with uncertainty ± 0.001, and for site- and pair-approximations of the master equations for this model. We also show the dependence of these estimates on various prescriptions of diffusion described in the text.

	Site approx.	Pair approx.	Simulation
Constant D	0.4420	0.4401	0.440
Modified	0.4249	0.4185	0.419
Diagonal (R)	0.4159	0.4062	0.406
Diagonal (C)	0.4175	0.4084	0.409
Exact (R)	0.4061	0.3945	0.395
Exact (C)	0.4078	0.3970	0.398

≈ 0.435, as might be expected for weakly clustered distributions.[30] With this revised estimate of q_c, we appropriately refine our description of CO-chemical diffusion. Specifically, we use the quadratic approximation for F_{perc} in terms of θ_{O}, but with an adjusted value of α so as to obtain the appropriate $q_c = 0.435$. We then reanalyze wave propagation and equistability. One could then continue to reassess percolation across the wave front, revise the treatment of CO-diffusion, reanalyze equistability, etc., until achieving self-consistency. However, to the level of precision used here, q_c does not change significantly from the first revised estimate of 0.435, and we obtain a final estimate of $p_{\text{CO}} \approx 0.398 \pm 0.001$ for the position of equistability point. We emphasize that this result is consistent with the value of $p^*(h \to \infty) = 0.397 \pm 0.002$ from Sec. II!

It is instructive to compare the above results for the equistability point in the hybrid model with those obtained from corresponding simulations with other (imprecise) treatments of diffusion. Results are shown in the right column of Table II for standard diffusion (constant D), for an approximate treatment based on Eq. (5) which underestimates the influence of coadsorbed O on CO-diffusion (Modified), for a correct treatment of $D_{\text{CO,CO}}$ *ignoring* the ''off-diagonal'' contribution due to $D_{\text{CO,O}} > 0$ (diagonal), and for the exact treatment according to Sec. III C (exact). In the latter two cases, we report results for random percolation with $q_c = 0.407 (R)$, and for correlated percolation with $q_c = 0.435$ (C). In addition, Table II shows corresponding results from a ''site-approximation'' and a ''pair-approximation'' to Eq. (9) and the associated hierarchy.[8] The former ignores all spatial correlations, and corresponds to a standard MF treatment, whereas the latter accounts for nearest-neighbor correlations. These results show that the prescription of diffusion does significantly influence the location of the equistability point, thus highlighting the importance of a correct treatment of diffusion. The results also show that the pair approximation provides an adequate treatment of spatial correlations in this hybrid model (cf. Ref. 8).

Simulations or approximate analytic treatments of the hybrid model can also be used to examine the variation of propagation velocity with p_{CO}, as well as the details of wave front structure. Figure 5 shows results for the scaled velocity, $v = V/h^{1/2}$, obtained from simulations of the full LG model

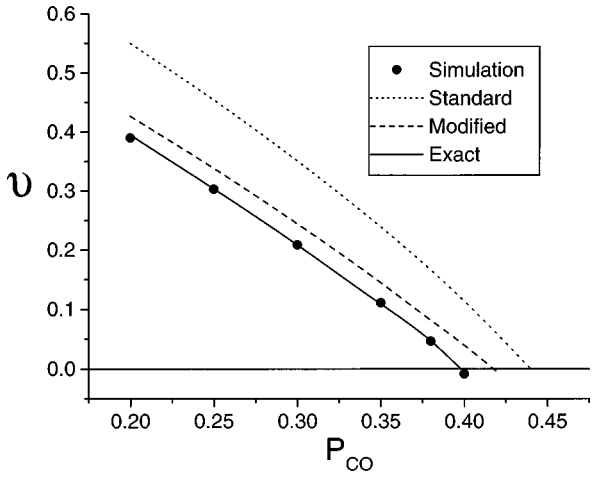

FIG. 5. Scaled propagation velocity, v, of the chemical wave, vs p_{CO}. Simulation results for the monomer–dimer LG model, with large $h = 512$, are compared with predictions from the hybrid treatment with various prescriptions of chemical diffusion.

with $h = 512$, compared against predictions of the hybrid model with various treatments of diffusion (and with the identification $D^0 = a^2 h$, where ''a'' is the lattice constant). Clearly a correct description of diffusion is necessary to quantitatively reproduce the value of the propagation velocity, as well as the equistability point. In Fig. 6(a), we show results for the coverage profiles across the stationary wave front at the equistability point obtained from the correct de-

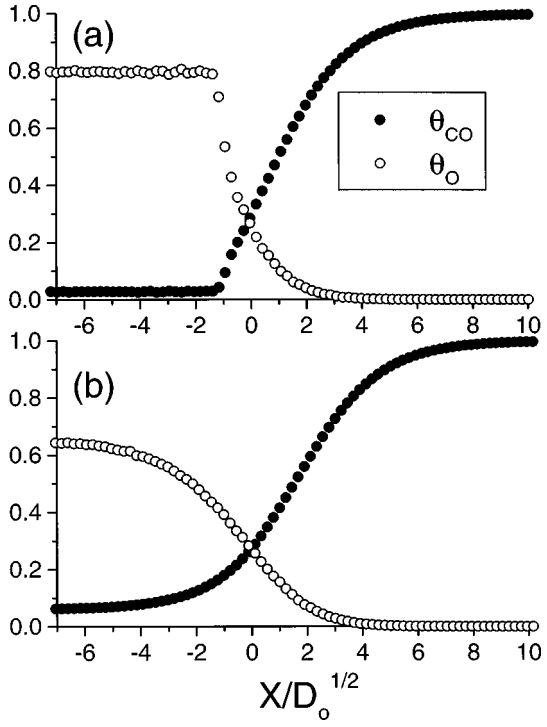

FIG. 6. Hybrid-model simulations for coverage profiles across the interface between the reactive steady-state (on the left) and the CO-poisoned state (on the right) at the equistability point (corresponding to the discontinuous transition, $p_{\text{CO}} = p^*$, in the LG model) for (a) percolative diffusion of CO; (b) standard diffusion of CO with constant D. Here we set $D_0 = D(\theta_{\text{O}} = 0)$.

scription of percolative diffusion. The shape of the profiles is very similar to that obtained from the LG simulations for large h shown in Fig. 3(c). On the other hand, the shape shown in Fig. 6(a) is quite distinct from the smooth form obtained using a conventional description of chemical diffusion with constant D, which is shown for comparison in Fig. 6(b).

V. MODEL REFINEMENTS AND COMPARISON WITH EXPERIMENT

We emphasize that the monomer–dimer surface reaction model, described above, provides an idealized description of CO-oxidation on surfaces. More realistic treatments might include a number of additional features, listed below as (i)–(v), which will modify the reaction kinetics, wave propagation features, and the chemical diffusion of CO(ads). Such refinements would be necessary for the type of detailed or quantitative comparison with experiment discussed at the end of this section.

(i) Nonreactive desorption of CO(ads) occurs under typical surface reaction conditions. With any such desorption, the completely CO-covered lattice is no longer a steady state. However, for realistically small desorption rates, the discontinuous transition persists in the LG model with finite h.[31] Also, bistability persists in the hydrodynamic regime, although the lower spinodal becomes a saddle-node bifurcation rather than a transcritical bifurcation. We emphasize, however, such desorption has no effect on the qualitative nature of chemical diffusion or wave propagation.

(ii) Reaction rate vs total adsorption rate. Often, the reaction rate is substantially larger than the total adsorption rate,[1] in which case there is less mixing of adsorbed reactants, and the description of diffusion becomes simpler. However, the case we consider where these rates are roughly equal is readily realized for higher pressures or somewhat lower temperatures.

(iii) Nonzero mobility of adsorbed O. Certainly O(ads) is not completely immobile under typical surface reaction conditions.[7] However, since the hop rate for the CO(ads) is undoubtedly far higher than that for O(ads), the picture of CO(ads) diffusing in a disordered quasistatic environment of coadsorbed O remains valid. The chemical diffusion of CO(ads) is still described as above, and controls spatiotemporal behavior. In contrast, for systems involving coadsorbed species with comparable high mobility, the description of chemical diffusion is distinct and more complicated.[32]

(iv) Adspecies interactions. Such interactions are invariably present and are usually significant, based on observed adlayer ordering and islanding. They directly affect adsorption and desorption kinetics,[1] and influence reaction kinetics through both direct and topological effects. Such interactions also produce coverage dependence in chemical diffusion in addition to that described above.[19]

(v) Adsorbate–substrate interaction. Experimental observations of CO-oxidation generally indicate that CO adsorption is possible on O-covered surfaces,[1] contrasting our model. This could, for example, be due distinct adsorption sites for CO(ads) and O(ads). A plausible consequence, of particular relevance for this study, is that diffusion of CO(ads) may *not* be as completely inhibited by coadsorbed O(ads) as in our treatment. Finally, we note that adsorbate-induced reconstruction of the substrate is also important in a number of reaction systems.[1] Recent studies[33] indicate that the microscopic picture can be substantially more complicated than envisaged in the original MF modeling,[1] which would also dramatically complicate LG modeling.

Next, we comment on experimental observations of chemical wave propagation during CO-oxidation, and on the relationship of this and other theoretical modeling to such observations. Photoemission electron microscopy (PEEM) studies have provided the most extensive data on chemical wave propagation, although these have not yet provided comprehensive data for V vs P_{CO} in simple bistable systems.[1] As a result, even the original MF modeling of wave propagation, motivated by these studies, was not able to make a direct comparison with experiment.[34] However, our study suggests one requirement for quantitative analyses of propagation velocities (from more extensive experimental data sets), and associated extraction of surface diffusivities. It is that such analyses should incorporate coverage dependence in chemical diffusion due to the interference of coadsorbed adspecies. Another message from our study is that observation of the full chemical wave front structure can provide insight into such nonlinearities. Unfortunately, PEEM does not have the resolution to discern such features, but this is possible with low energy electron microscopy,or mirror electron microscopy.[35]

VI. SUMMARY

We have analyzed chemical wave propagation in a lattice-gas monomer–dimer surface reaction model for CO-oxidation, with finite reaction rate and with various degrees of CO-mobility. A ''near-crossing'' feature of the propagation velocity curves versus a measure of CO-partial pressure allows precise estimation of the position of the equistability point for reactive and CO-poisoned in the physically relevant limiting regime of high CO-mobility. (This point corresponds to the CO-poisoning transition in the LG model.) This estimate is consistent with a direct treatment of wave propagation in this limiting regime, within a ''hydrodynamic'' reaction-diffusion formalism, using a hybrid approach of Ref. 8, only with a correct description of CO-diffusion. Here it is necessary to account for the percolative nature of CO chemical diffusion, and for the feature that coverage gradients in the immobile coadsorbed O induce a diffusive flux of CO. The traditional description of diffusion with coverage independent D produces significant errors in the propagation velocity and equistability point. We also find

that the shape of the wave profile close to the CO-poisoning transition is sensitive to the percolative nature of CO-diffusion, and is quite distinct from predictions with coverage-independent D.

ACKNOWLEDGMENTS

This work was supported by the Division of Chemical Sciences, Office of Basic Energy Sciences, of the U.S. Department of Energy (USDOE). It was performed at Ames Laboratory, which is operated for the USDOE by Iowa State University under Contract No. W-7405-Eng-82.

APPENDIX A: MONOMER–DIMER MODEL WITH INSTANTANEOUS REACTION

Goodman *et al.*[10] analyzed chemical wave propagation for the monomer–dimer reaction model with *infinite* k, but retaining mobile CO(ads) with hop rate h, and immobile O(ads). A ''near-crossing'' of V vs p_{CO} curves, for different h, was first observed in this model. Since the location of the CO-poisoning transition, $p^*(h)$, as well as $dV/d\Delta$, *increases* with h, the ''crossing point'' occurs for $p_{CO}=p_x$ *above* $p^*(h)$. Just as for the case $k=1$, one can exploit this ''near-crossing'' behavior to estimate.

$$p^*(h\to\infty)=p_x\approx 0.574\pm 0.004, \text{ for inifinite } k. \quad \text{(A1)}$$

The exact value is actually $p^*(h\to\infty)=4/7\approx 0.5714$.[36] This result agrees with the prediction of Ref. 11 that p^* should increase with h from $p^*(0)=0.526$ to a value strictly below 2/3, and contrasts earlier claims.[37]

Note that wave propagation for $p_{CO}>p^*$ (up to p_{s+}) corresponds to displacement of the stable CO-poisoned state by the metastable reactive state, and thus only occurs until the latter poisons. Wave propagation is not well-defined for $p_{CO}>p_{s+}$. For $k=\infty$, V vs p_{CO} curves must be extended into this ''metastable propagation'' regime above p^* in order to reach the ''crossing point.'' This is not even possible for small $h<9/4$, where $p_{s+}<p_x$, but it is readily achieved in practice for larger h where $p_{s+}>p_x$, due to strong metastability.

APPENDIX B: FLUCTUATIONS AT THE CHEMICAL WAVE FRONT

As noted in Sec. III C, the fluctuations in the location of the interface include both intrinsic and long-wavelength contributions. Precise definition of the former is generally vague. For $p_{CO}<p^*$, where the long-wavelength fluctuations are of the KPZ-type, the amplitude, ξ_i, of the intrinsic fluctuations can in principle be extracted from the total amplitude, ξ, for a system of width L, from the asymptotic slope of $\xi^2/L\approx\xi_i^2/L+\gamma/(24v)$ vs $1/L$.[16] On the other hand, in the regime of large h of interest here, the intrinsic fluctuations dominate on the characteristic length scale $L\sim h^{1/2}$ (recalling that $v\sim h$). Some insight into the behavior of ξ_i in this regime comes from the analysis of ''diffusion fronts'' in nonreactive systems.[38] Here it has been shown that the amplitude of fluctuations at the diffusion front (defined as the ''seashore'' of the diffusing species) scales like $(d\theta/dx)^{-4/7}$, where $d\theta/dx$ denotes the concentration gradient at the front. For our system, this gradient scales like $h^{-1/2}$, which suggests that $\xi_i\sim h^{2/7}$. As an aside, we note that Goodman *et al.*[10] used the term ''intrinsic width'' in their study, which corresponded to our characteristic length, $L_c\sim h^{1/2}$, rather than to $\xi_i\sim h^{2/7}$.

TABLE III. Estimates of thresholds, q_c, for percolation of non-O(ads) or Z-sites, obtained using various RG prescriptions, and from more ''exact'' procedures. Results are shown for randomly distributed O(ads) (random percolation), for RSA of O_2(gas) dimers, and for the hybrid model scanning states across the reaction front near the equistability point. In the latter two cases, we show the estimated shift, δ, in q_c due to correlations, and refine the RG estimates of q_c using $q_c(\text{revised})\approx 0.4073+\delta$.

	Random O(ads)	RSA of O_2(gas)	Hybrid model
$R_Z(b=3)=\theta_Z$	0.3807	0.420 ($\delta=0.039$)	0.425 ($\delta=0.044$)
$R_Z(b=3)=1/2$	0.4407	0.466 ($\delta=0.025$)	0.469 ($\delta=0.028$)
$R_Z(b=2)=R_Z(b=3)$	0.379	0.400 ($\delta=0.021$)	0.422 ($\delta=0.043$)
Exact	0.4073	0.434 ($\delta=0.027$)	⋯

APPENDIX C: WAVE PROPAGATION ABOVE THE POISONING TRANSITION

We consider the LG monomer–dimer reaction model with $k=1$ and finite h, and for p_{CO} slightly above the poisoning transition in the range $p^*<p_{CO}<p_{s+}$. Here the reactive steady-state is metastable, and since the value of θ_O in this state exceeds q_c, diffusive coupling of the CO-poisoned state to the metastable reactive state is inhibited. On the other hand, direct spatial coupling between these states always exists due to reaction of neighboring CO and O adspecies. Thus, the CO-poisoned state does displace the metastable reactive state, creating a chemical wave, at least until the latter spontaneously poisons. In fact, extensive ''local diffusion'' of CO(ads) generally occurs from the CO-poisoned state into the ''frontier'' of the reactive state, and thus we find that the interface propagation velocity and structure at first vary conventionally with increasing h. However, for large enough h, the inhibited diffusive coupling must control behavior as discussed in Sec. IV B. A detailed analysis will be reported elsewhere.

We have noted in Sec. II A that spatially inhomogeneous versions of ''dynamic cluster'' approximations to the master equations do incorporate the direct spatial coupling due to reaction.[20,21] Thus, they do predict chemical wave propagation both above and below the equistability point, which corresponds to the discontinuous poisoning transition. However, clearly such approximations cannot describe the complicated local diffusion of CO(ads) mentioned above, as this requires a precise characterization of the connectivity of non-O(ads) or Z-sites at the frontier of the reactive state.

APPENDIX D: REAL-SPACE RG ANALYSIS OF PERCOLATION

Consider lattice-gas systems with a continuous family of states in which each site is designated by either O or Z, and where these states are uniquely labeled by the coverage of

Z-sites, θ_z, or of O-sites, $\theta_O = 1 - \theta_z$. Real-space renormalization group (RG) techniques can be applied as follows to assess whether the Z-sites percolate.[29] One determines the probability, R_z, that $b \times b$ site cells to span the cell horizontally (say), as a function of the corresponding θ_z. Standard criteria considered here for the threshold, $\theta_O = 1 - \theta_z = q_c$, above which the Z-sites cease to percolate include $R_z(b=3) = \theta_z$; $R_z(b=3) = 1/2$; or $R_z(b=2) = R_z(b=3)$. Table III shows the results for q_c applying these criteria for randomly distributed O(ads), for irreversible random sequential adsorption (RSA) of O_2(gas) dimers on adjacent sites of a square lattice,[25] and for the O(ads) distribution in states scanning the reaction front near equistability in the hybrid treatment of the monomer–dimer reaction model. Using RSA as a benchmark, it appears that estimates for correlated O(ads) distributions of the *shift*, δ, in q_c from its value for random percolation are more accurate than direct estimates of the actual value of q_c. Thus we refine direct estimates of q_c using q_c (random percolation) $+\delta = 0.4073 + \delta$. Furthermore, the criteria $R_z = 1/2$ appears to provide the most reliable estimate of δ for RSA. Also it was recently shown to be most appropriate for random percolation,[39] and thus is used for our analysis in Sec. IV of the hybrid model.

[1] R. Imbihl and G. Ertl, Chem. Rev. **95**, 697 (1995).
[2] V. P. Zhadanov and B. Kasemo, Surf. Sci. Rep. **20**, 111 (1994); J. W. Evans and M. Sabella, Trends Stat. Phys. **1**, 107 (1994); J. W. Evans, Langmuir **7**, 2514 (1991).
[3] R. M. Ziff, E. Gulari, and Y. Barshad, Phys. Rev. Lett. **50**, 2553 (1986).
[4] M. Dumont, P. Dufour, B. Sente, and R. Dagonnier, J. Catal. **122**, 95 (1990).
[5] J. W. Evans and M. S. Miesch, Phys. Rev. Lett. **66**, 833 (1991).
[6] J. W. Evans and T. R. Ray, Phys. Rev. E **50**, 4302 (1994).
[7] E. G. Seebauer and C. E. Allen, Prog. Surf. Sci. **49**, 265 (1995).
[8] M. Tammaro, M. Sabella, and J. W. Evans, J. Chem. Phys. **103**, 10277 (1995).
[9] D. S. Sholl, and R. T. Skodje, Surf. Sci. **334**, 295 (1995).
[10] R. H. Goodman, D. S. Graff, L. M. Sander, P. Leroux-Hugon, and E. Clement, Phys. Rev. E **52**, 5904 (1995).
[11] J. W. Evans, J. Chem. Phys. **98**, 2463 (1993).
[12] R. M. Ziff and B. J. Brosilow, Phys. Rev. A **46**, 4630 (1992).
[13] Note that h in Ref. 8, and Γ in Ref. 9, denote the total hop rate for CO(ads), rather than the hop rate per direction (as used here). Results in this paper are not quantitatively consistent with those in Ref. 9 for p^* vs Γ.
[14] V also decreases linearly with Δ in the monomer–dimer model with infinite k (see Refs. 6, 10). However a nonlinear decrease applies approaching a continuous poisoning transition (Ref. 6).
[15] D. Mollison, J. R. Stat. Soc. B **39**, 283 (1977).
[16] J. Kertesz and D. E. Wolf, J. Phys. A **21**, 747 (1988).
[17] J. Krug and H. Spohn, in *Solids Far From Equilibrium*, edited by C. Godreche (Cambridge University Press, Cambridge, 1991).
[18] A. S. Mikhailov, *Introduction to Synergetics I* (Springer, Berlin, 1990).
[19] R. Gomer, Rep. Prog. Phys. **53**, 917 (1990).
[20] P. Fischer and U. M. Titulaer, Surf. Sci. **221**, 409 (1989).
[21] D. S. Sholl and R. T. Skodje, Surf. Sci. **334**, 305 (1995).
[22] R. Kutner, Phys. Lett. A **81**, 239 (1981).
[23] The classic analysis of Kutner (Ref. 22) for a noninteracting lattice-gas on a perfect lattice can be readily extended to the case of a (static) disordered lattice. See R. Kutner and K. W. Kehr, Philos. Mag. A **48**, 199 (1983); C. H. Mak, H. C. Andersen, and S. M. George, J. Chem. Phys. **88**, 4052 (1988).
[24] D. Stauffer and A. Aharony, *Introduction to Percolation Theory* (Taylor & Francis, London, 1992); *Fractals and Disordered Systems*, edited by A. Bunde and S. Havlin (Springer, Berlin, 1991).
[25] J. W. Evans, Rev. Mod. Phys. **65**, 1281 (1993).
[26] Th. M. Nieuwenhuizen, P. J. F. van Veltoven, and M. H. Ernst, Phys. Rev. Lett. **57**, 2477 (1986); J. Phys. A **20**, 4001 (1987).
[27] M. Silverberg and A. Ben-Shaul, J. Chem. Phys. **87**, 3178 (1989); K. A. Fichthorn and W. H. Weinberg, Langmuir **7**, 2539 (1991).
[28] Equation (9) shows that the slope discontinuity, $[d/d\xi\theta_{CO}(0+) - d/d\xi\theta_{CO}(0-)]$ must be matched by the $\xi = 0+$ value of $-V^{-1}d/d\xi[D_{CO,CO}d/d\xi\theta_{CO} + D_{CO,O}d/d\xi\theta_O]$, which is proportional to $F'_{perc}(p_c)$. The exact value of $F'_{perc}(p_c)$ is zero since the critical exponent $\mu > 1$, but its value is nonzero it does occur using a quadratic approximation.
[29] H. E. Stanley, P. J. Reynolds, S. Redner, and F. Family, in *Topics in Current Physics*, edited by T. W. Burkhardt and J.M. J. van Leeuwen (Springer, Berlin, 1982), Vol. 30; P. J. Reynolds, H. E. Stanley, and W. Klein, Phys. Rev. B **21**, 1223 (1980).
[30] D. E. Sanders and J. W. Evans, Phys. Rev. A **38**, 4186 (1988).
[31] B. J. Brosilow and R. M. Ziff, Phys. Rev. A **46**, 4534 (1992); T. Tome, and R. Dickman, *ibid.* **47**, 948 (1993); J. W. Evans and M. Sabella, in Ref. 2.
[32] M. Tammaro and J. W. Evans, Surf. Sci. Lett. (to be published).
[33] A. Hopkins, J. M. Bradley, X.-C. Guo, and D. A. King, Phys. Rev. Lett. **71**, 1597 (1993).
[34] M. Bar, Ch. Zulicke, M. Eiswirth, and G. Ertl, J. Chem. Phys. **96**, 8595 (1992).
[35] W. Swiech, C. S. Rastomjee, R. Imbihl, J. W. Evans, B. Rausenberger, W. Engel, A. K. Schmid, A. M. Bradshaw, and E. Zeitler, Surf. Sci. **307/309**, 138 (1994).
[36] M. Tammaro and J. W. Evans, Phys. Rev. E (submitted).
[37] H. P. Kaukonen and R. M. Nieminen, J. Chem. Phys. **91**, 4380 (1989); M. Ehsasi, M. Matloch, J. H. Block, K. Christmann, F. S. Rys, and W. Hirschwald, *ibid.* **91**, 4949 (1989).
[38] J.-F. Gouyet, M. Rosso, and B. Sapoval, in *Fractals and Disordered Systems*, edited by A. Bunde and S. Havlin (Springer, Berlin, 1981).
[39] R. M. Ziff, Phys. Rev. Lett. **69**, 2670 (1992); **72**, 1942 (1994).